Cellular Oncology (2025) 48:1299–1315
https://doi.org/10.1007/s13402-025-01066-5

RESEARCH

Synthetic NKG2D receptor (SNR) armored CAR-T cells overcome antigen heterogeneity of solid tumor

Minmin Sun[1,2,3,4] · Linke Bian[5,6] · Hongye Wang[5,6] · Xin Liu[1] · Yantao Li[3,4] · Zhaorong Wu[5,6] · Shuangshuang Zhang[3,4] · Ruidong Hao[3,4] · Hong Xin[1] · Bo Zhai[7] · Xuemei Zhang[1,2] · Yuanguo Cheng[1,2,3]

Received: 8 January 2025 / Accepted: 21 April 2025 / Published online: 19 June 2025

Abstract

Background CAR-T cell therapy has demonstrated remarkable success in hematologic malignancies; however, its effectiveness against solid tumors remains limited due to tumor antigen heterogeneity. NKG2DLs, including MICA/B and the ULBP family, are stress-induced molecules frequently upregulated on the surface of tumor cells and components of the tumor microenvironment, providing attractive targets for immunotherapy. To broaden the targeting capability beyond conventional Claudin18.2-directed CAR-T cells, we engineered a Synthetic NKG2D Receptor (SNR). The SNR comprises the extracellular domain of NKG2D fused with the intracellular signaling domains of DAP10 and DAP12, enabling effective targeting of NKG2D ligands (NKG2DLs).

Methods Expression of NKG2DLs and CLDN18.2 were detected by immunohistochemistry on a gastric cancer tissue microarray. We designed SNR CAR-T cells by linking CLDN18.2 CAR with SNR by a 2A self-cleaving peptide. We assessed their cytotoxicity, tumor infiltration, persistence, and antitumor efficacy using in vitro assays, patient-derived xenograft (PDX) models, and murine syngeneic models. Additionally, transcriptomic analysis and flow cytometry were performed to evaluate exhaustion and memory markers.

Results SNR CAR-T cells demonstrated enhanced cytotoxicity against tumor cells with heterogeneous CLDN18.2 expression, effectively lysing both CLDN18.2-positive and NKG2DL-positive tumor cells in vitro. In PDX and murine models, SNR CAR-T cells exhibited superior antitumor efficacy, leading to significant tumor regression and CAR-T expansion compared to conventional CAR-T cells. Furthermore, SNR CAR-T cells displayed reduced expression of exhaustion markers and increased expression of memory-associated markers. Enhanced tumor infiltration, proliferation and cytotoxicity within the tumor microenvironment, and a reduced presence of myeloid-derived suppressor cells (MDSCs) and tumor neovasculature were observed. Importantly, SNR CAR-T cell therapy was well-tolerated, with no significant toxicity noted in all the treated animals.

Conclusion The SNR CAR-T cell approach addresses tumor antigen heterogeneity and suppressive tumor microenvironment, offering a promising therapeutic strategy for solid tumors and paving the way for its future clinical applications.

Keywords NKG2D · NKG2D ligands · Chimeric antigen receptor · Tumor antigen heterogeneity · Solid tumor

1 Introduction

Chimeric antigen receptor (CAR) T-cell therapy has revolutionized cancer treatment, providing a targeted approach that redirects immune cells to specifically recognize and eliminate tumor cells [1]. This therapy has shown remarkable efficacy in hematological malignancies, where CARs are engineered to target antigens such as CD19 or B-cell maturation antigen (BCMA) [2, 3]. However, translating CAR-T cell therapies to solid tumors presents significant challenges, one of which is the heterogeneity in tumor antigen expression [3, 4]. T cell cytotoxicity relies on

Minmin Sun, Linke Bian, and Hongye Wang Contributed equally to this work.

Extended author information available on the last page of the article

precise receptor-ligand binding, and the bystander effect of CAR-T therapy is not pronounced [5]. After CAR-T treatment, tumor cells with low or absent antigen expression could re-expand and become the dominant clones, leading to tumor recurrence [6, 7].

Claudin 18.2 (CLDN18.2), a member of the tight junction protein family, has emerged as a promising tumor associated antigen (TAA) for solid tumor therapy, with high expression levels in gastric cancer (GC), gastroesophageal junction (GEJ) cancers and pancreatic cancers (PC) [8–10]. In normal tissues, CLDN18.2 is restricted to gastric mucosal, without expression on any other tissues [8, 9]. Various therapeutic modalities targeting CLDN18.2 have been developed, including antibodies, antibody drug conjugates (ADC), bispecific T cell engager (BiTE), and CAR-T [9]. Among these modalities, autologous CLDN18.2 CAR-T has shown a favorable objective response rate (ORR) of 57.1% and disease control rate (DC) of 75% in patients with GC [11]. However, only patients with CLDN18.2 staining more than 40% in tumor samples were eligible for this treatment [11], which represents less than 30% of GC patients [10, 12–14]. In clinical trials of zolbetuximab monotherapy in GC, only patients with CLDN18.2 staining higher than 70% benefited from the treatment [15, 16]. These studies indicate that expression heterogeneity of CLDN18.2 might restrict the efficacy of CLDN18.2 targeting therapy, and the development of novel therapy to address it is warranted to benefit more patients.

NKG2D (Natural Killer Group 2, Member D) is an activating receptor expressed on the surface of various immune cells, including natural killer (NK) cells, CD8+T cells, and certain subsets of CD4+T cells [17–19]. It plays a crucial role in the immune system. by recognizing NKG2D Ligands (NKG2DLs). NKG2DLs are stress-induced proteins including MICA, MICB, and ULBP (UL16 binding proteins) family members in humans [20, 21]. NKG2DLs are widely expressed in various solid and hematologic cancers [22, 23]. In normal tissues, NKG2DL expression is generally low or absent, thereby preventing unintended immune activation. However, certain conditions can induce NKG2DL expression in healthy cells. For instance, MICA and MICB are constitutively expressed on normal intestinal epithelial cells, likely due to stimulation by the gut's bacterial flora. Additionally, NKG2DLs can be upregulated on activated immune cells; for example, ULBP1 expression is induced during normal myeloid differentiation and on monocytes and granulocytes in peripheral blood from healthy donors.

The binding of NKG2D to its ligands triggers cytotoxicity against target cells through the adaptor protein DNAX-activating protein 10 (DAP10) in CD8+T cells [17], whereas in NK cells, it can pair with DAP10 in human or, in mice DAP10 and its homolog DAP12 [24]. In CD8 T cells, DAP10 recruits p85 to induce PI3K signaling and Grb2 to activate Vav-SOS signaling, leading to repression of T-bet and upregulation of Bcl-2, which result in enhanced cell survival and memory formation [18, 25–27]. DAP12 contains an immunoreceptor tyrosine-based activation motif (ITAM) that, upon phosphorylation, recruits and activates Syk and ZAP70 tyrosine kinases [28, 29]. DAP12-based NKG2D CAR has shown lower cytokine secretion and comparable cytotoxicity to conventional CAR signaling [30]. Recent studies, notably by Obajdin et al. [33], demonstrated that the combined DAP10-DAP12 structure within an NKG2D-based adaptor CAR provides superior antitumor efficacy compared to conventional CAR designs (NKG2D-CD3ζ). Their research revealed that incorporating both DAP10 and DAP12 signaling domains enhances oxidative phosphorylation, reduces T cell senescence, and facilitates transcriptional reprogramming toward increased ribosomal biogenesis, collectively contributing to sustained T cell persistence and robust antitumor responses.

To address tumor antigen heterogeneity of GC, we first detect CLDN18.2 and NKG2DLs expression on GC tissues and PDX tumors treated with conventional CLDN18.2 CAR-T. NKG2DLs were ubiquitously expressed on GC tissues and remained highly expressed after treatment. Then, we designed a dual-targeting strategy that combines the activating receptor NKG2D with the conventional CLDN18.2 CAR, termed Synthetic NKG2D Receptors CAR-T (SNR CAR-T). The SNR is composed of the extracellular domain of NKG2D and the signaling domain of DAP10 and DAP12. Our results demonstrate that SNR CAR-T cells exhibit enhanced antitumor activity in both in vitro and in vivo models with homogenous or heterogeneous CLDN18.2 expression. SNR was shown to improve CAR-T memory formation and reduce exhaustion. In the syngeneic model, SNR was able to reduce tumor neovasculature, MDSC and leading to enhanced antitumor efficacy. Collectively, our results suggested that SNR is a promising strategy for the treatment of advanced gastric and pancreatic cancer.

2 Results

2.1 Heterogeneous CLDN18.2 expression in solid tumors highlights need for NKG2D-targeting strategies

The heterogeneous expression of CLDN18.2 might restrict the efficacy and application of its targeting therapies. To investigate the potential of dual targeting to enlarge the target spectrum, we evaluated the expression of CLDN18.2 and NKG2D ligands (NKG2DLs), including ULBP1, ULBP2/3/5/6, and MICA/B, in a gastric cancer tissue array.

Results showed that CLDN18.2 is positively expressed in 38% of gastric cancer tissues. Moreover, the staining pattern observed is patchy, with regions showing low or no expression of CLDN18.2. (Fig. 1A–B). Two of NKG-2DLs, ULBP1, and ULBP4, were almost expressed in all the gastric tissues, whereas other NKG2DLs, MICA/B and ULBP2/5/6, exhibit variable expression (Fig. 1A). Importantly, we observed that NKG2DLs were expressed in tissues lacking CLDN18.2 expression (Fig. 1A-B). These results support the rationale for employing NKG2DLs and CLDN18.2 dual-targeting approach with CAR-T cells.

We then developed a conventional second-generation CAR-T cell targeting human CLDN18.2 to investigate the impact of antigen heterogeneity on CAR-T efficacy. The CLDN18.2 CAR construct includes a humanized VHH recognizing both murine and human CLDN18.2, a human CD28 hinge, transmembrane and the endo-cellular domain, and the intracellular domain of human CD3ζ (Fig. 2A). These CLDN18.2 CAR-T cells exhibited potent and specific cytotoxicity against both human and murine CLDN18.2-positive cells in vitro (Supplementary Fig. 1 A-F). Additionally, in an immunocompromised mouse model bearing NUGC4-Luc tumors with high CLDN18.2 expression, CLDN18.2 CAR-T cells effectively eliminated tumors (Supplementary Fig. 1 G-I). Moreover, CLDN18.2 CAR-T cells resulted in significant antitumor effects in a patient-derived xenograft (PDX) model of gastric cancer (Fig. 1C-D). Immunohistochemical analysis of PDX tumors post-treatment revealed a decreased CLDN18.2 expression. We also observed that NKG2DLs maintained high and homogenous expression patterns in the tumor tissues across different groups (Fig. 1E). These findings collectively underscore the potential of co-targeting NKG2DLs as a strategy to augment the efficacy of conventional second-generation CAR-T.

2.2 SNR CAR-T cells showed enhanced in vitro cytotoxicity against tumors with heterogeneous CLDN18.2 expression

Based on our findings indicating that simultaneous targeting of CLDN18.2 and NKG2D ligands (NKG2DLs) might broaden CAR-T cell recognition in gastric cancer, we

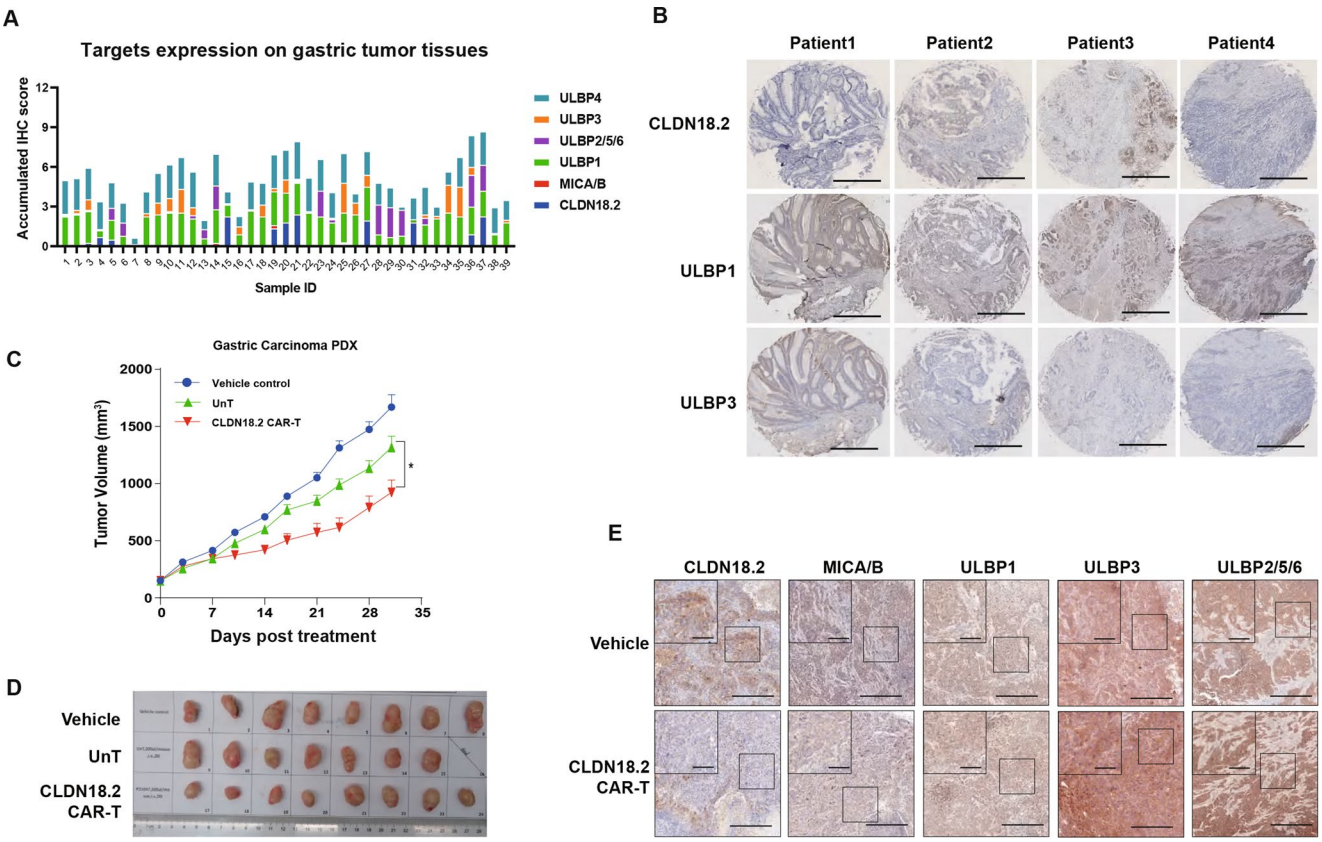

Fig. 1 CLDN18.2 was heterogeneously expressed in gastric cancer tissues. (**A**) Histogram of accumulative IHC score of CLDN18.2 and NKG2DLs in microarray of gastric cancer. HC scores (H-score) were calculated by multiplying staining intensity (scored as 0 [no staining], 1+ [weak], 2+ [moderate], and 3+ [strong]) by the percentage of positive cells, resulting in a score ranging from 0 to 300. (**B**) Representative immunohistochemistry images of gastric carcinoma tissues. 5x magnification (**C**) Tumor volume change in gastric carcinoma PDX model. Values are presented as mean± SEM. (**D**) Representative images of tumors in each group at D35. (**E**) Representative images of immunohistochemistry on tumor tissues at the endpoint of the PDX experiment (10x and 20x magnification)

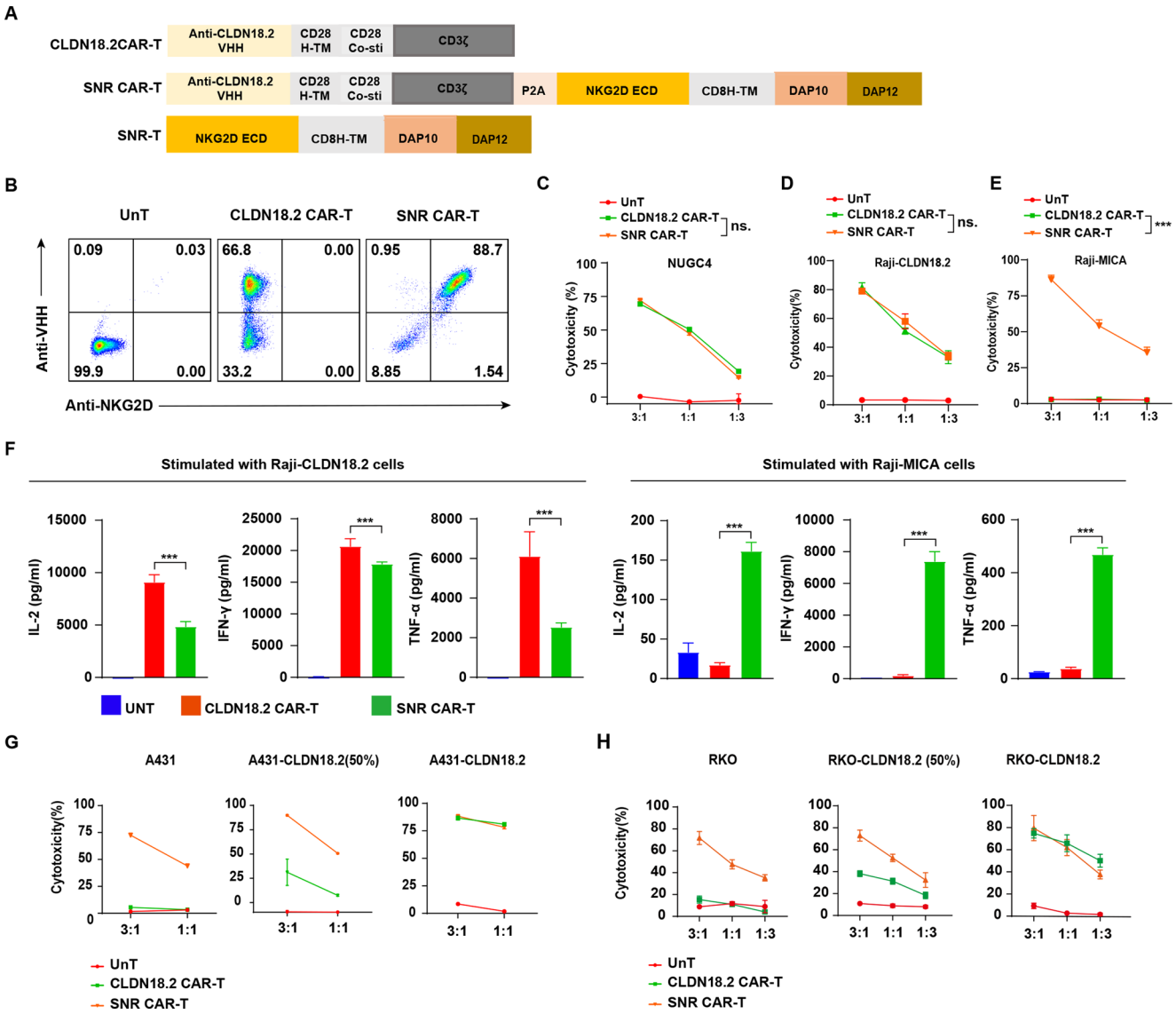

Fig. 2 SNR-CAR-T could target multiple cancer cells in vitro. (**A**) Schematic construction of CLDN18.2 CAR-T and SNR CAR-T. (**B**) Expression of CAR and NKG2D were analyzed by flow cytometry. (**C**) Cytotoxicity of UNT, CLDN18.2 CAR-T, and SNR CAR-T against gastric cell line NUGC4-Luc, CLDN18.2 overexpressed Raji cell line (**D**) and MICA overexpressed Raji cell line (**E**) at varying target: effector ratio. (**F**) Multiple cytokines secretion was measured after CAR-T co-culturing with Raji-CLDN18.2 or Raji-MICA at the effector: target ratio of 1:1 for 12 h. (**G**) Cytotoxicity of CLDN18.2 CAR-T and SNR CAR-T against multiple tumor cell lines derived from A431. (**H**) Cytotoxicity of CLDN18.2 CAR-T and SNR CAR-T against multiple tumor cell lines derived from RKO. Values are presented as mean ± SD

developed a synthetic NKG2D receptor (SNR). SNR incorporates the intracellular signaling domains of DAP10 and DAP12 with the extracellular domain of NKG2D. The SNR construct was then fused to the CLDN18.2 CAR using a 2A self-cleaving peptide, creating SNR CAR-T cells (Fig. 2A). The co-expression of CAR and SNR was verified by flow-cytometry (Fig. 2B). To further assess the efficacy of SNR CAR-T cells, we employed the human gastric cancer cell line NUGC4-Luc, which endogenously expresses CLDN18.2. Co-culture experiments with NUGC4-Luc cells confirmed that both CLDN18.2 CAR-T and SNR CAR-T cells were capable of efficiently lysing CLDN18.2-positive target cells (Fig. 2C). Raji cells are negative for both CLDN18.2 and NKG2DLs, and we overexpressed CLDN18.2 or MICA in these cells (Fig. 2A-D). Upon stimulation with Raji-CLDN18.2 cells, both conventional and SNR CAR-T cells could lyse target cells and secret high levels of cytokines IL-2, TNFα, and IFN-γ (Fig. 2D-F). However, when co-cultured with Raji-MICA cells, only SNR CAR-T cells exhibited enhanced cytotoxicity against Raji-MICA and produced moderate levels of IL-2, TNFα, and IFN-γ as expected (Fig. 2E-F).

To evaluate the dual-targeting capability of SNR CAR-T cells, we utilized CLDN18.2-negative RKO (human colon

carcinoma cell line) and A431 (human epidermoid carcinoma) cell lines, which naturally express high levels of NKG2DLs (Supplementary Fig. 2 C). We constructed double-positive RKO and A431 cells for CLDN18.2 and NKG2DLs by overexpressing CLDN18.2 (Supplementary Fig. 2 A). Then we mixed them with their parental lines to generate 50% CLDN18.2-positive and 100% NKG2DL-positive cell lines to mimic the antigen heterogeneity of tumor tissue. As expected, only SNR CAR-T cells were able to eliminate the parental cells A431 and RKO (Fig. 2G and H). Although SNR-CAR-T and conventional CAR-T showed comparable cytotoxicity against A431-18.2 and RKO-18.2, the SNR-CAR-T demonstrated significantly higher killing efficiency against mixture cells with 50% CLDN18.2 expression (Fig. 2G and H). These results underscore the potential of SNR CAR-T cells to target tumor cells with heterogenous CLDN18.2 expression.

2.3 SNR CAR-T cells exhibit a stronger memory phenotype and reduced exhaustion

We then investigated the effects of SNR on the cellular phenotypes of CLDN18.2 CAR-T cells by transcriptome sequencing. Under the resting condition without antigen engagement, bulk RNA sequencing analysis revealed a downregulation of genes associated with T cell exhaustion (EOMES, CD160, LAG3, CTLA4, NFATC4, TOX2) and activation (TNFRSF9, TNFSF9, IL2RA, CD69, CD38, TNFSF4) in SNR CAR-T cells. Concurrently, upregulation of genes related to T cell memory (TCF7, SELL, CD27, CNR2, PDE9A, CTSC, LEF1) was observed in SNR CAR-T cells (Fig. 3A). Gene Set Enrichment Analysis (GSEA) corroborated these findings, indicating that SNR CAR-T cells exhibit a reduced state of exhaustion and heightened memory formation even in the absence of stimulation (Fig. 3A).

One possible explanation for these phenotypic changes in SNR CAR-T cells under resting conditions is the presence of tonic signaling or fratricide. The NKG2D/DAP10-12 structure used in SNR CAR-T has been shown to promote persistent but controlled signaling in T cells. Recent findings by Obajdin et al. (Cell Rep Med. 2024) demonstrated that CARs utilizing a similar NKG2D/DAP10-12 adaptor structure exhibit enhanced oxidative phosphorylation, reduced senescence, and transcriptomic reprogramming, leading to increased ribosomal biogenesis. These metabolic adaptations may contribute to the observed memory phenotype in SNR CAR-T cells even in the absence of external antigen stimulation. While tonic signaling can sometimes drive exhaustion in conventional CAR-T constructs, the SNR CAR appears to maintain a favorable balance, sustaining T cell persistence without excessive activation.

In line with the transcriptome analysis, we examined the proportion of Stem cell-like memory T (Tscm) cells, which are known for their robust antigen-dependent proliferation capabilities. Our data indicate a notable increase in the Tscm subsets of both CD4 and CD8 positive cells in SNR CAR-T compared to CLDN18.2 CAR-T cells (Fig. 3B). Flow cytometry measurements of additional T cell memory and exhaustion markers further confirmed the transcriptomic findings, with SNR CAR-T cells displaying increased expression of memory-associated marker CD27, CD62L and TCF7, and reduced expression of the exhaustion marker PD-1 (Fig. 3C-3D).

Utilizing CyTOF (cytometry by time of flight), we further resolved the phenotypic profile of CAR-T cells in the resting state (Fig. 3E). The SNR CAR-T cells exhibited elevated levels of CD62L and CD45RA (Fig. 3F and G), consistent with the flow cytometry results. In contrast, SNR CAR-T cells demonstrated reduced expression of activation and exhaustion markers: CD25, CD38, CD39, and PD1 (Fig. 3F). Notably, a subset of CD8 positive cells with high levels of CD39 and CD56, indicative of dysfunctional or terminally exhausted T cells with inhibitory potential, was observed in conventional CAR-T cells but not in SNR CAR-T cells (Fig. 3F). Similarly, a subset of CD4 positive cells with high expression of CD25 and PD1, typically associated with an exhausted phenotype, was less prevalent in SNR CAR-T cells.

Collectively, these findings suggest that SNR CAR-T cells possess an enhanced memory phenotype and a reduced exhausted state, which may contribute to their in vivo persistence and anti-tumor efficacy.

2.4 SNR CAR-T cells enhanced the antitumor efficacy in xenograft models with homogenous CLDN18.2 expression

Our initial in vivo evaluation of SNR CAR-T cells utilized the NUGC4-Luc cell line, a human gastric cancer model that endogenously expresses CLDN18.2 and NKG2DLs. We established xenograft tumors in immunodeficient mice and treated them with CLDN18.2 CAR-T or SNR CAR-T cells. Remarkably, both CAR-T cell treatments demonstrated potent tumor control, with the SNR CAR-T group exhibiting a significantly lower tumor volume, resulting in complete tumor regression in all mice (Fig. 4A). This enhanced therapeutic effect was without increased toxicity, as evidenced by the stable body weight and absence of adverse effects in the treated mice (Fig. 4B).

We then extended our investigation to the MIAPaCa2-CLDN18.2 models, which was a pancreatic cancer cell line genetically modified to stably express CLDN18.2 and endogenously express NKG2DLs (Supplementary Fig. 2

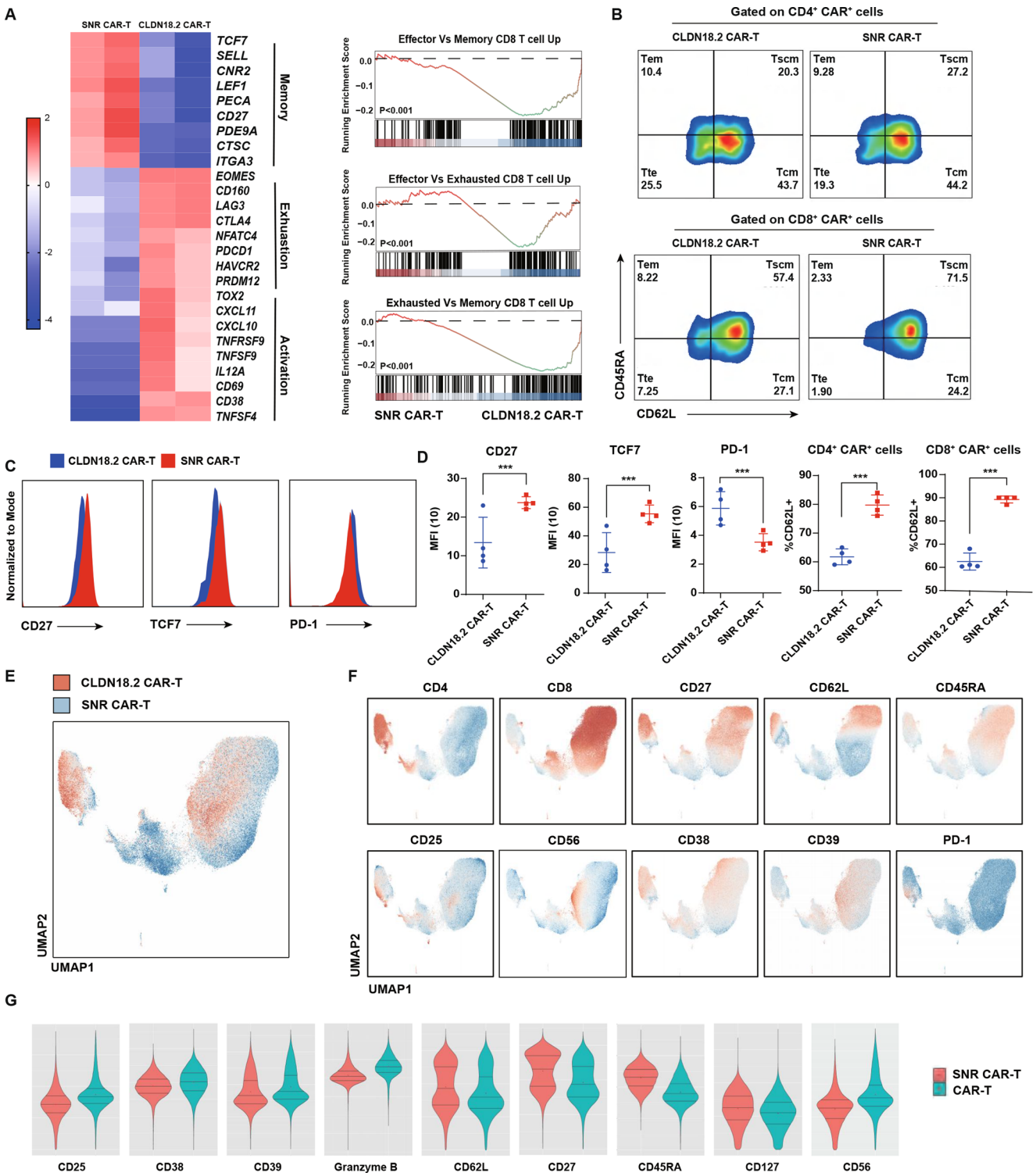

Fig. 3 SNR-CAR-T promotes CAR-T potency in memory differentiation and reduces exhaustion. (**A**) CLDN18.2 CAR-T and SNR CAR-T cells under resting status without antigen engagement were analyzed with transcriptional sequencing. Heatmap displayed the differentially expressed genes (DEGs) related to different T cell phenotypes. Gene set enrichment analysis (GSEA) of key phenotype related pathways between CLDN18.2 CAR-T and SNR CAR-T cells. (**B**) The proportion of different subsets of CLDN18.2 CAR-T and SNR CAR-T cells after stimulated with NUGC4-LUC cells for 3 days. (**C**) CD27, TCF7 and PD-1 expression in CAR-T and SNR CAR-T cells was measured with flow cytometry. (**D**) Mean fluorescence intensity (MFI) of CD27, TCF7 and PD-1 from four independent donors. Percentage of CD62L+T cells in CLDN18.2 CAR-T and SNR CAR-T cells. (**E**) UMAP plot of total cell population grouped by CLDN18.2 CAR-T and SNR CAR-T cells. (**F**) UMAP plots of key T cell phenotype markers. (**G**) Relative expression of key T cell phenotype markers between CLDN18.2 CAR-T and SNR-CAR T cells. Values are presented as mean± SD

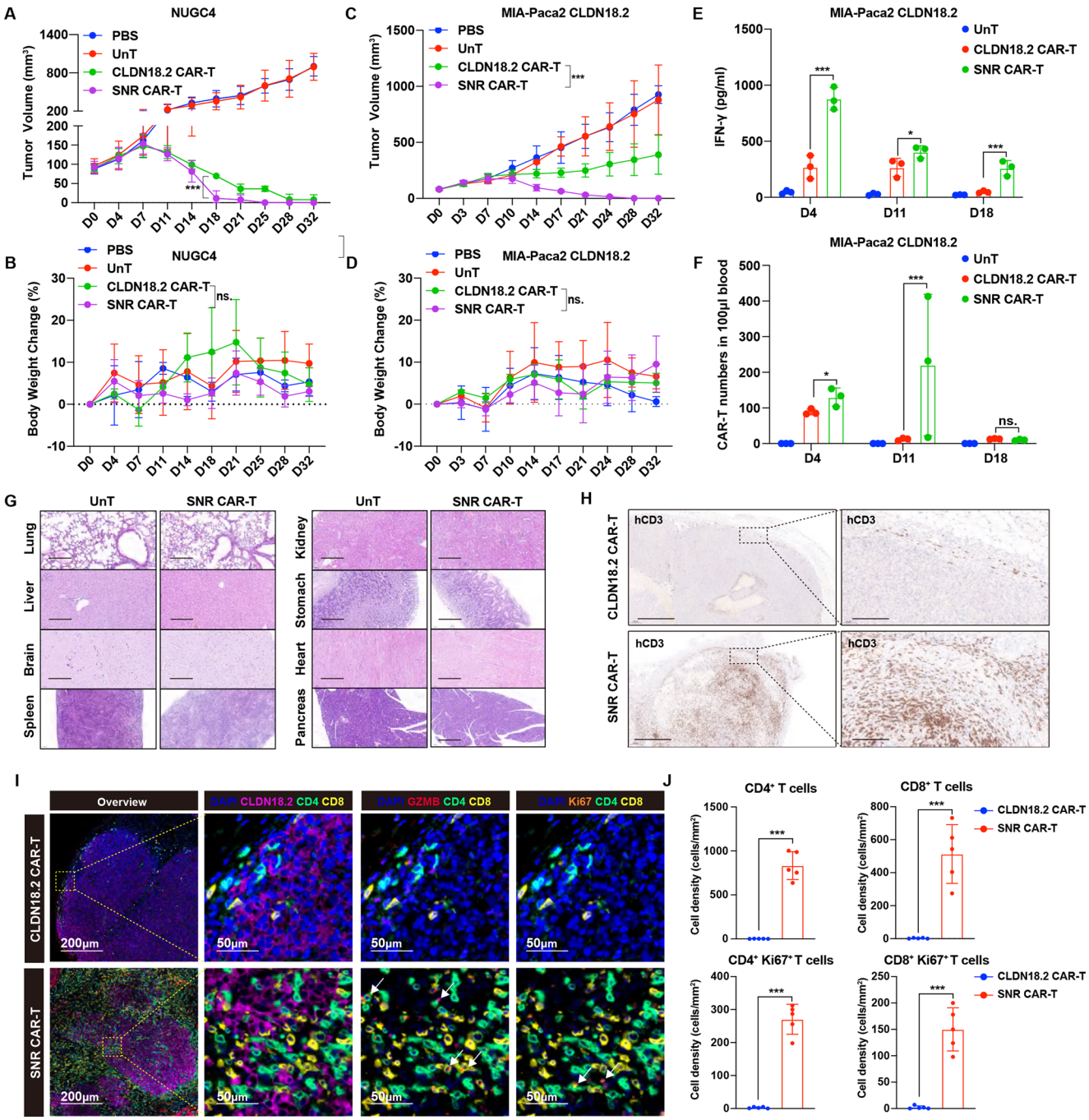

Fig. 4 SNR-CAR- T cell improved CLDN18.2-dependent antitumor efficacy and infiltration in homogeneous xenograft models. NUGC4-Luc CDX models (**A**) Tumor volume and (**B**) Body weight changes at indicated days were monitored. (**C**–**G**) CLDN18.2 overexpressed MIA-Paca2 CDX models (**C**) tumor volume and (**D**) body weight change at indicated days was monitored. (**E**) IFN-γ of peripheral blood was detected at indicated days with ELISA. (**F**) The absolute number of CAR-T in 100 μL blood were detected at indicated days after CAR-T infusion. (**G**) Representative images of H&E staining of different organs following SNR CAR-T or UNT infusion in CLDN18.2 overexpressed MIA-Paca2 CDX models. (5x magnification). (**H**) The MIA-Paca2-CLDN18.2 tumors were analyzed by IHC for T cell infiltration (anti-human CD3). Scale bars stand for 500 μm and 50 μm. (**I**) mIHC staining was performed to investigate the infiltration and status of tumors treated with CLDN18.2 CAR-T or SNR CAR-T cells. (**J**) Statistics data of CD4, CD8, CD4 + Ki67 +, CD8 + Ki67 + cell counts in tumors from each mouse. Values are presented as mean ± SD

B&C). Notably, in this pancreatic cancer xenograft model, SNR-CAR-T showed significantly higher antitumor efficacy than CLDN18.2 CAR-T, leading to complete tumor eradication in all mice (Fig. 4C). A significantly higher level of IFN-γ secretion and CAR-T expansion were noted in the SNR-CAR-T group (Fig. 4E&F). SNR-CAR-T was well tolerated in this model as evidenced by body weight and pathology examination (Fig. 4D&G).

To further investigate the contribution of SNR to the antitumor efficacy of SNR-CAR-T, the MIAPaCa2-CLDN18.2 models were treated by SNR-T, CLDN18.2 CAR-T, or SNR-CAR-T. Results showed that SNR-T has minimal antitumor efficacy. The tumors were eradicated in 1 of 5 mice treated by CLDN18.2 CAR-T, and 3 of 5 mice treated by SNR-CAR-T. Only the SNR-CAR-T group is statistically different from the untransduced T cells (UNT) treated control group. These results suggested a potential synergistic effect between SNR and CAR arm in the SNR-CAR-T (Supplementary Fig. 2 C).

2.5 SNR CAR-T showed higher infiltration in immune-excluded tumors

To probe the mechanisms underlying the superior antitumor activity of SNR CAR-T cells, we assessed the infiltration and status of CAR-T in the MIA PaCa2-CLDN18.2 xenograft models. By IHC staining for human CD3, we analyzed the presence of CAR-T cells in MIA-Paca2 tumor xenografts. In the CLDN18.2 CAR-T treated group, the T cell infiltration displayed a typically immune-excluded form, as they were confined to the stroma and seldom infiltrated into the tumor nest (Fig. 4H). In contrast to the immune-excluded pattern observed in the CLDN18.2 CAR-T treated group, mice treated with SNR CAR-T cells displayed extensive T cell infiltration throughout the tumor mass (Fig. 4G). This enhanced tumor infiltration was further confirmed by multiplex IHC (mIHC) co-staining with a panel of immune markers, including CLDN18.2, human CD4, CD8, GZMB, and the proliferation marker Ki67 (Fig. 4I). The Ki67 and GzmB staining revealed increased proliferative and cytotoxicity of SNR CAR-T cells within the tumor microenvironment (Fig. 4I and J). These findings highlight the ability of SNR CAR-T cells to infiltrate into excluded tumors, leading to more effective antitumor activity.

2.6 Overcoming antigen heterogeneity with SNR CAR-T in tumor models

To address the challenge of antigen heterogeneity in tumors in vivo, we developed a murine model that mimics the complexity of human cancer. By mixing CLDN18.2-negative but NKG2DLs-high parental A431 cells with CLDN18.2-overexpressing A431 cells in a 7:3 ratio, we created a tumor with 30% CLDN18.2 expression. In this model, SNR CAR-T cells exhibited a significant inhibitory effect on tumor growth (Fig. 5B) and were associated with a notable expansion of T cells at day 9 post-treatment (Fig. 5C). In contrast, CLDN18.2 CAR-T cells were ineffective in controlling tumor growth and failed to expand following infusion (Fig. 5C). To translate our findings to more clinically relevant settings, we evaluated the efficacy of SNR CAR-T cells in a patient-derived xenograft (PDX) model alongside the conventional CAR-T cells. Immunohistochemical analysis of the PDX tumor samples revealed an uneven expression pattern of CLDN18.2, and a strong and homogenous staining of certain NKG2DLs (Fig. 1E). In this model, both types of CAR-T cells were potent in controlling tumor growth; however, SNR CAR-T cells showed a trend towards more effective T cell expansion and superior control of tumor growth (Fig. 5e–f). These results suggested that SNR-CAR-T has higher antitumor efficacy against tumors with heterogenous CLDN18.2 expression.

2.7 Murine SNR improves the efficacy of CAR-T with a good safety profile in syngeneic models

We further evaluated the efficacy and safety of SNR CAR-T cells in immunocompetent mice using a syngeneic Panc02 model that overexpresses mouse claudin18.2. To this end, we first constructed and validated murine CLDN18.2 CAR-T cells and murine SNR CAR-T cells based on murine T cells in vitro (Fig. 6A). Panc02 is a well-recognized immune-excluded mouse pancreatic ductal adenocarcinoma model. In the in vivo experiments, SNR CAR-T cells demonstrated a modest (Reviewer1, Question 8) antitumor effect (Fig. 6B, c). Both the SNR-CAR-T and conventional CAR-T were well tolerated in this model, without causing body weight loss or abnormalities in general observation or premature death (Fig. 6D). Tissue samples from critical organs including kidney, lung, spleen, liver, heart, stomach, Intestine, and skin were resected and subjected to H&E staining and pathological inspection. HE staining results showed that both CLDN18.2 and SNR CAR groups exhibited mild inflammatory infiltration (mainly neutrophils) only in lung and stomach tissues, without any tissue or cell damage observed (Fig. 6E). Collectively, these results demonstrate that murine SNR could improve the efficacy of conventional CAR-T without causing additional toxicity.

Studies have reported that NKG2D ligands are highly expressed on the surface of tumor neovasculature, and targeting NKG2DLs may disrupt tumor blood vessels, affecting tumor nutrient and oxygen supply, thus inhibiting tumor growth [31]. Additionally, NKG2DLs are highly expressed in MDSC cells, and targeting them could

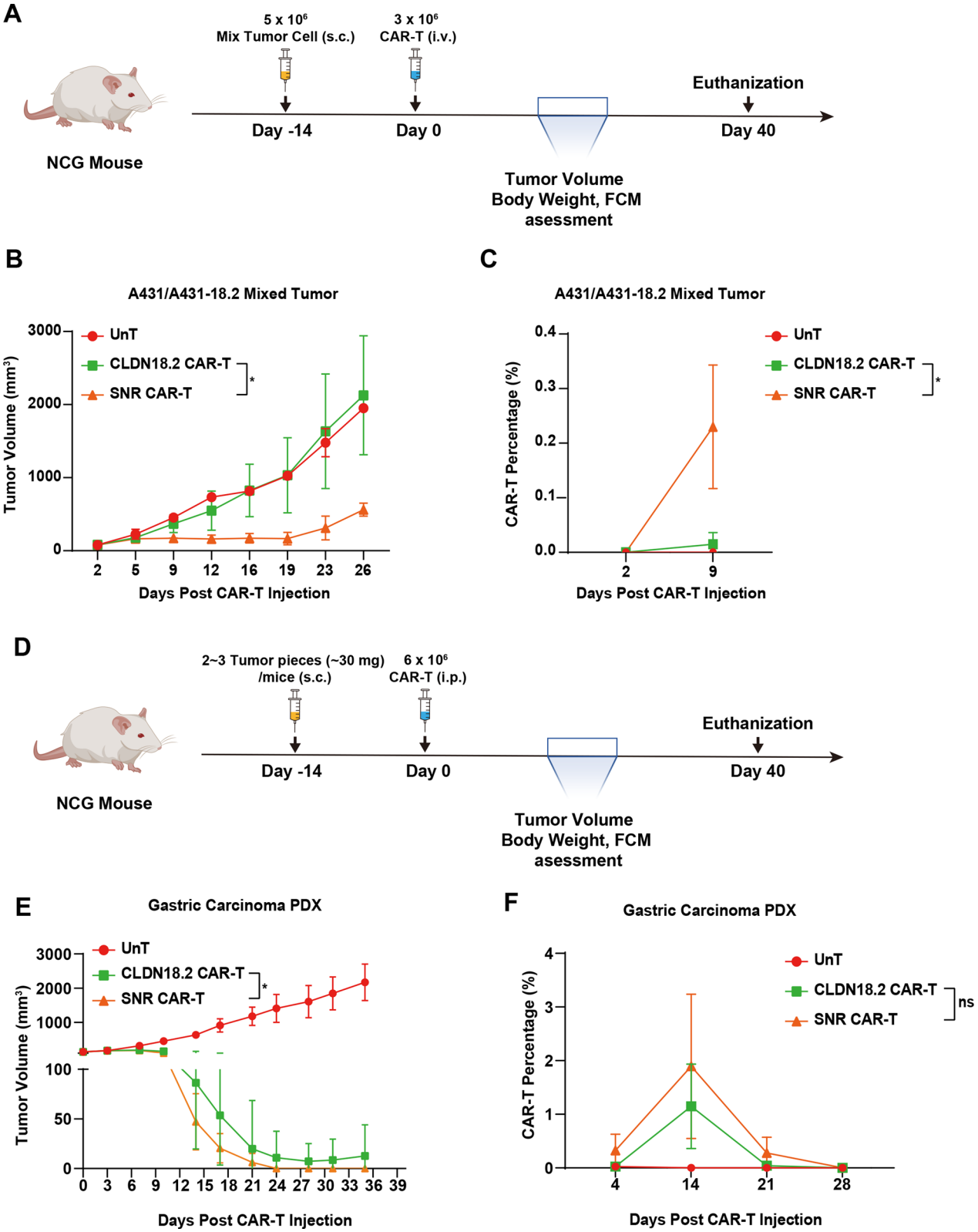

Fig. 5 SNR CAR-T had a superior antitumor effect against tumors with heterogeneous CLDN18.2 expression in vivo. (**A**–**C**) A431 and A431- CLDN18.2 were mixed at a 7:3 ratio to generate A431 CDX model ($n=5$) (**B**) the tumor volume changes were recorded and (**C**) the CAR-T percentages in peripheral blood at 2 or 9 days after CAR-T infusion were analyzed with flow cytometry. (**D**–**E**) Gastric Carcinoma PDX model ($n=5$). (**E**) Tumor volume was measured and (**F**) CAR-T percentage in peripheral blood was detected after CAR-T infusion. Values are presented as mean ± SEM

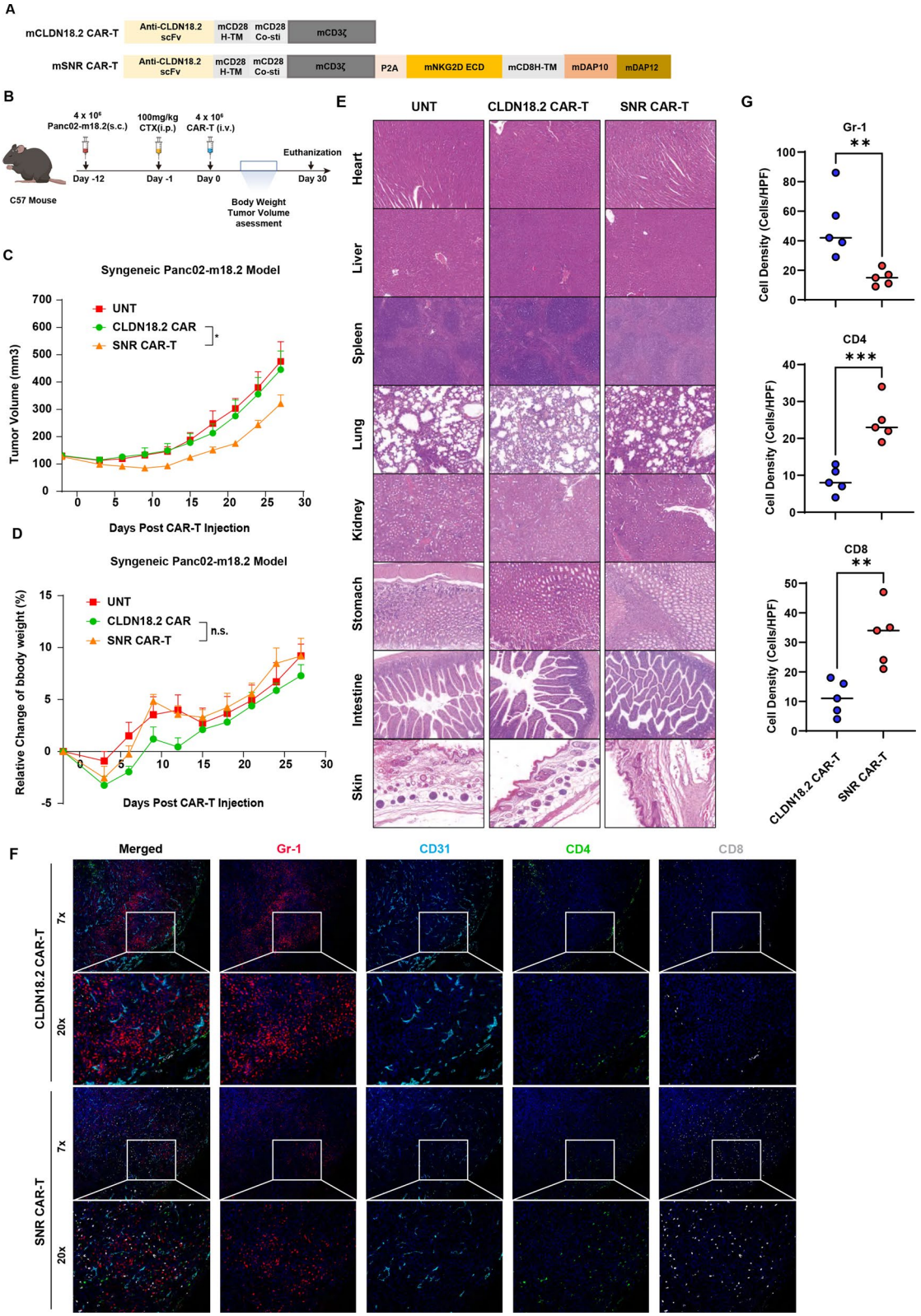

alleviate the immunosuppressive environment caused by MDSCs, thereby increasing T-cell infiltration [31, 32]. At the end of the experiment, we performed mIHC on tumor tissues to observe and quantify CD4, CD8, CD31, and Gr-1 markers (Fig. 6F, G). The results showed that compared to CLDN18.2 CAR-T cells, SNR CAR-T cells showed

Fig. 6 SNR CAR-T demonstrated superior efficacy and acceptable safety in immunocompetent mouse models. (**A**) Schematic construction of mCLDN18.2 CAR-T and mSNR CAR-T. The efficacy and safety of murine SNR CAR-T cells were evaluated in murine CLDN18.2 over-expressed syngeneic Panc02 models ($n=5$). Twelve days after inoculation with 5 × 106 Panc02 cells, lymphodepletion was induced with an intraperitoneal injection of 100 mg/kg cyclophosphamide (CTX) (**B**). Twenty-four hours later, 4 × 106 CAR-positive cells were administered via tail vein injection. Tumor volume changes (**C**) and body weight changes (**D**) were recorded for each group of mice. On day 30 post-CAR-T injection, organs from each group of mice were collected for HE staining (**E**). Simultaneously tumor tissues were collected from each group of mice for Multiplex-IHC staining (7x magnification) (**F** and **G**). Values are presented as mean ± SEM

significantly reduced Gr-1 positive myeloid cells, increased CD8 T cell infiltration, and changed CD4 T cell infiltration from the tumor margins into the tumor core. Additionally, the quantity and thickness of tumor blood vessels marked by CD31 decreased. Collectively, these results suggest SNR-CAR-T could overcome suppressive TME by inhibiting angiogenesis and MDSC in tumors.

3 Discussion

CLDN18.2 has emerged as a promising therapeutic target for advanced gastric and pancreatic cancers, and various treatment strategies have been developed. Among these, autologous CAR-T therapies targeting CLDN18.2 demonstrated significant responses in gastric cancer patients with high antigen expression. However, patients with low CLDN18.2 expression (<40%) were typically excluded from clinical trials, creating uncertainty regarding the efficacy of CLDN18.2 CAR-T therapy in this subgroup. Additionally, the limited effectiveness of CAR-T therapy in pancreatic cancer is likely due to the immunosuppressive and cold tumor microenvironment (TME), characterized by restricted T cell infiltration. These challenges underscore the need for strategies that address antigen heterogeneity and the suppressive TME.

Our study addresses these limitations by developing a synthetic NKG2D receptor (SNR) designed to target broadly expressed NKG2D ligands (NKG2DLs), including MICA/B and ULBP family members, which are widely expressed in various solid and hematopoietic malignancies, including gastric and pancreatic cancer. Consistent with previous studies, our findings indicate universal expression of at least one NKG2DL in gastric cancer tissues, in contrast to the heterogeneous expression of CLDN18.2. The dual-targeting approach of SNR CAR-T cells effectively broadens antigen recognition beyond CLDN18.2, thus potentially overcoming the issue of antigen heterogeneity.

The SNR construct integrates the extracellular domain of NKG2D with the intracellular signaling domains DAP10 and DAP12, offering several advantages over conventional CAR constructs. Recent research by Obajdin et al. validated that CAR constructs using the NKG2D/DAP10-12 structure exhibit superior efficacy compared to traditional NKG2D-CD3ζ CARs [33]. Specifically, this configuration promotes enhanced oxidative phosphorylation, reduces T cell senescence, and induces transcriptomic reprogramming for increased ribosomal biogenesis, resulting in improved CAR-T persistence and sustained tumor control. Our results align with these findings, show that SNR CAR-T cells exhibit transcriptional and proteomic signatures associated with enhanced memory formation and reduced exhaustion. Transcriptome analyses revealed significant upregulation of memory-associated genes such as TCF7, LEF1, and SELL, alongside downregulation of exhaustion markers including LAG3, CTLA-4, and PDCD1. This memory phenotype aligns with the known functions of NKG2D-DAP10 signaling in promoting T cell survival, persistence, and differentiation into memory cells.

Our in vitro studies demonstrated that SNR CAR-T cells selectively eliminate tumor cells expressing NKG2DLs with moderate cytokine secretion, while maintaining comparable cytotoxic efficacy with reduced cytokine release when targeting CLDN18.2-positive cells. Importantly, in cell line-derived xenograft (CDX) and patient-derived xenograft (PDX) models simulating antigen heterogeneity, SNR CAR-T exhibited superior antitumor efficacy and greater tumor cell killing compared to conventional CLDN18.2 CAR-T cells.

Our syngeneic mouse model studies, employing mouse NKG2D targeting mouse NKG2DLs, allowed for accurate evaluation of efficacy and potential on-target, off-tumor toxicities associated with NKG2D signaling in an immunocompetent setting, given the known lack of cross-reactivity between human NKG2D and mouse ligands [34]. SNR CAR-T cells demonstrated effective tumor control and maintained an acceptable safety profile, with no significant toxicity observed. Additionally, SNR CAR-T treatment reduced tumor neovasculature and myeloid-derived suppressor cell (MDSC) infiltration, potentially facilitating enhanced intratumoral CD8 + T cell infiltration and cytotoxic activity. Thus, SNR CAR-T cells not only broaden antigen targeting but also reshape the suppressive TME, enhancing overall antitumor efficacy.

Our study has limitations, in some of our experiments, the absence of a dedicated control group expressing SNR alone without the CLDN18.2 CAR, limiting our ability to clearly attribute observed enhancements in memory phenotype and reduced exhaustion solely to SNR signaling. Another limitation is the absence of data addressing the impact of soluble forms of NKG2DLs, such as soluble MICA/B (sMICA/sMICB), on the effector functions of SNR

CAR-T cells. Tumor cells can shed these ligands through proteolytic cleavage, potentially reducing CAR-T efficacy through competitive inhibition. Additionally, our study did not assess the effector function of SNR CAR-T cells across cell lines with varying expression levels (different mean fluorescence intensities, MFI) of CLDN18.2, representing another limitation. Our in vivo evaluation of SNR CAR-T cells was limited to short-term murine models, which may not fully capture potential chronic toxicities or delayed adverse reactions observed in clinical settings. Long-term follow-up studies are essential to assess the persistence of CAR-T cells and the risk of late-onset toxicities, such as prolonged cytopenias and hypogammaglobulinemia. Additionally, differences in NKG2D ligand distribution between mice and humans may limit the translatability of our findings. Future research should incorporate long-term studies and consider species-specific differences to better evaluate the safety profile of SNR CAR-T cells.

Our results suggest that the universal co-targeting capability provided by the NKG2D/DAP10-12 structure in SNR CAR-T cells represents a promising approach to address tumor antigen heterogeneity and TME-driven immunosuppression. Further preclinical validation and clinical trials are warranted to optimize this strategy for clinical application.

4 Conclusions

Our SNR CAR-T system represents a significant advancement in solid tumor therapy by targeting both CLDN18.2 and NKG2DLs. This approach has the potential to improve T cell memory and expand the in vitro and in vivo efficacies against tumors with varying antigen expression. Further studies are warranted to fully characterize and clinically develop this novel therapeutic strategy.

5 Methods

5.1 Cell culture

Human skin cancer cell line A431 and gastric cancer cell line NUGC4-luc were obtained from MODEL ORGANISMS Co., Ltd (Shanghai, China), while Raji, MIA-Paca2, and RKO cells were sourced from the American Type Culture Collection (ATCC, Manassas, VA, USA). These cell lines were selected for their natural deficiency in CLDN18.2 expression. CLDN18.2-overexpressing variants were generated by transfecting these cells with VSV-G pseudotyped lentivirus encoding full-length human CLDN18.2. Tumor cells were cultured in Dulbecco's Modified Eagle's Medium (DMEM; Life Technologies) supplemented with 10% FBS (Gibco), 100 mg/mL penicillin, and 100 mg/mL streptomycin sulfate (Gibco) at 37 °C with 5% CO2. Raji cells were cultured in RPMI 1640 (Gibco) under the same conditions. All cell lines were authenticated using Short Tandem Repeat (STR) analysis by Shanghai Biowing Applied Biotechnology (Shanghai, China).

5.2 Human T cell isolation and CAR-T construction

CD3-positive T cells were isolated from peripheral blood mononuclear cells (PBMCs) using CD3 magnetic beads (Miltenyi Biotech). The isolated T cells were cultured in X–vivo (Lonza) medium supplemented with 5% FBS (Gibco), 100 mg/mL penicillin, 100 mg/mL streptomycin sulfate (Gibco), and 300 IU/mL IL-2 (Peprotech). CD3+T cells were stimulated with 10 μg/mL anti-CD3 and anti-CD28 antibodies (Novoprotein) in six-well plates coated with RetroNectin (TaKaRa). A previously developed VHH targeting human CLDN18.2 with high specificity was used, derived from patent PCT/CN2022/105029. The CAR construct, consisting of the anti-CLDN18.2 VHH, human CD8α hinge, transmembrane domain, and cytoplasmic co-stimulatory CD28 and CD3ζ signaling domains, was inserted into a third-generation lentiviral vector driven by the EF1α promoter. After 24 h, activated T cells were infected with the lentivirus at a multiplicity of infection (MOI) of 10, and transduction rates were assessed using flow cytometry with an anti-VHH antibody (Genscript) 72 h post-activation. The VHH and ScFv sequence used in the paper is provided in Supplementary Table 2.

5.3 Primary mouse T cell isolation and CAR T-cell production

For T cell activation, 6-well plates were pre-coated with 5 ml of anti-CD3 (0.5 μg/ml, Clone: 2C11) and anti-CD28 (5 μg/ml, Clone: 37.51) at 4 °C for 18 h. T cells were isolated using a mouse CD3 positive selection kit (Biolegend) and then plated onto the pre-coated wells at 5×10^6 cells per well in 5 ml of complete medium (RPMI supplemented with penicillin/streptomycin, 10% FBS, 1x NEAA, 1x sodium pyruvate, 1× 2-mercaptoethanol, and 1x ITS [Insulin-Transferrin-Selenium, Thermo Fisher]). The cells were cultured undisturbed at 37 °C for 48 h. Twenty-four hours prior to transduction, plates that had not been treated were coated with 15 μg/ml of novonectin (Novoprotein). On the second day, cells were harvested, counted, and resuspended at 2×10^6 cells/ml in complete medium supplemented with 20 μg/ml of polybrene and 40 IU/ml of mIL-2. Novonectin-coated plates were blocked with 0.05% FBS in PBS for 30 min before use. Each well of the blocked novonectin plates received 1 ml of virus supernatant, followed by the

addition of 1 ml of cell suspension. The mixture was gently shaken to achieve a working concentration of polybrene at 10 μg/ml and mIL-2 at 20 IU/ml. Spin infection was performed at 2000 x g for 120 min at 32 °C. The plates were then transferred to an incubator and maintained overnight. On day 3, plates were briefly centrifuged at 1000 x g for 1 min, and the virus-containing supernatants were carefully removed. Fresh complete medium with 20 IU/ml of mIL-2 was added to each well. Cells were passaged at a 1:2 ratio every 24 h with fresh medium containing 20 IU/ml of mIL-2. Transduction efficiency was assessed by surface staining with an anti-mouse Fab antibody (Jackson ImmunoResearch) targeting the murine scFv in the CAR construct approximately 48 h after transduction. If necessary, CAR T-cells could be frozen on day 3 for future assays following flow cytometry analysis of virus transduction. For in vivo experiments, CAR T-cells were utilized on day 6, whereas in vitro experiments continued until day 7.

5.4 Clone construction, retrovirus production and transduction

The murine CLDN18.2 CAR (m28z) and SNR CAR constructs were cloned into an MSCV retroviral vector, as described previously. For optimal retrovirus production, 293 Plat-E Eco cells were cultured to 80% confluence and subsequently split at a 1:2 ratio for further expansion. After 24 h, 5.6×10^6 cells were seeded in a 10 cm dish and cultured for an additional 16 h until reaching 70% confluence. One hour prior to transfection, each 10 cm dish was replenished with 10 ml of pre-warmed medium. Transfection was performed using the calcium phosphate method, following the manufacturer's protocol (Clontech). Specifically, for each transfection, 18 μg of plasmid DNA (comprising 16.2 μg of CAR plasmid and 1.8 μg of Eco packaging plasmid) was mixed with 610 μl of distilled water, followed by the addition of 87 μl of 2 M $CaCl_2$. Subsequently, 700 μl of DMEM medium was added dropwise with gentle vortexing. After a 10-min incubation at 25 °C, the transfection mixture was gently added to the PlatE-Eco cells. Following a 30-min incubation at 37 °C, the formation of fine particles was confirmed, indicating successful transfection. The next day, the medium was carefully removed and replaced with 8 ml of pre-warmed medium, without disturbing the cells. Virus-containing supernatant was collected 36 h later, filtered through a 0.45 μm filter to remove cell debris, aliquoted, and stored at − 80 °C. The virus transduction efficiency was evaluated in a 12-well format by mixing 0.5 million activated T cells with 0.5 ml of virus from each batch. Plate coating, spin infection, and FACS analysis of CAR expression were performed as previously described. The VHH and ScFv sequence used in the paper is provided in Supplementary Table 2.

5.5 In vitro cytotoxicity and cytokine secretion assays

CAR-T cytotoxicity was assessed by detecting annexin-V positive tumor cells after co-culture with CAR-T cells using fluorescence-activated cell sorting (FACS). Tumor cell lines were stained with carboxyfluorescein succinimidyl ester (CFSE) and cultured in X–vivo medium supplemented with 5% FBS and 1% penicillin-streptomycin (Thermo) before co-culture with CAR-T cells at various effector: target ratios. After 5 h, cells were stained with APC-Annexin-V and analyzed by FACS. Cytokine secretion was measured in cell culture supernatants using the LEGENDplex Human Th1 Panel (BioLegend).

5.6 Flow cytometry

Flow cytometry was performed on 2×10^5 cells, which were harvested, washed with PBS, and incubated with antibodies at a 1:500 dilution for 20 min at room temperature. The transduction rate of lentivirus on CAR-T cells was determined using a FITC-anti-VHH antibody (GenScript Inc.). Target cells were analyzed for NKG2D ligands using anti-MICA/MICB and anti-ULBP2/5/6 antibodies. CAR-T cell phenotypes were assessed using antibodies against CD25, CD69, CD62L, CD45RA, PD-1, and CD27 (Biolegend).

5.7 RNA sequencing

Conventional and SNR CAR-T cells were sorted and expanded for 7 days post-transfection. Total RNA was isolated using the RNA minikit (Qiagen, Germany) and assessed for quality using gel electrophoresis and Qubit (Thermo, Waltham, MA, USA). Strand-specific libraries were prepared using the TruSeq RNA Sample Preparation Kit (Illumina, SanDiego, CA, USA), and sequencing was performed on the Illumina Novaseq 6000 instrument (GenergIo technology Co.Ltd, Shanghai, China). Data were processed using Skewer and Fast QC v0.11.2. Clean reads were aligned to the human genome hg38 using STAR, and transcript expression was quantified by TPM (Transcripts Per Million) using Perl. Differentially expressed genes (DEGs) were identified using the MA-plot-based method with Random Sampling (MARS) and the DEGseq package. Enrichment analysis for DEGs was performed using the Gene Ontology (GO) and KEGG databases.

5.8 Hematoxylin and Eosin (HE) staining

The isolated organ tissues were fixed in 4% paraformaldehyde at room temperature for 24 h. Following fixation, the tissues were washed with phosphate-buffered saline (PBS) and embedded in paraffin. The embedded tissues were then sectioned into several μm thick slices. These sections were stained with hematoxylin and eosin using standard protocols. Each tissue section was examined under a light microscope, and five non-overlapping fields of view were randomly selected for observation.

5.9 Immunohistochemical (IHC) assay

IHC analysis was performed on a D046St01 microarray containing 40 cases of gastric adenocarcinoma and 6 cases of adjacent gastric tissue (Bioaitech Co., Ltd). The IHC procedure involved sectioning, dewaxing, blocking, and staining with primary antibodies overnight at 4 °C. Staining intensity and distribution were scored semi-quantitatively, and the IHC score was calculated by multiplying the percentage of positive cells by the staining intensity score. The gastric cancer and paracancer tissue microarrays used in this experiment were commercial tissue microarrays purchased from Bioaitech Co.

5.10 Multiplex immunohistochemistry (mIHC) assay

The experiment begins by fixing tumor samples in formalin, followed by embedding the fixed tissue samples in paraffin and sectioning them. Next, the paraffin sections are deparaffinized in xylene and rehydrated through a series of graded ethanol solutions. Antigen retrieval is then performed. Subsequently, the sections are incubated with an appropriate blocking solution to prevent nonspecific binding. The first primary antibody is then applied, typically incubating overnight at 4 °C. Detection of the primary antibody is achieved using a fluorescently labeled secondary antibody, and images are captured using a fluorescence microscope. Fluorescence signal removal agents are then used to eliminate the fluorescence signal, preparing the sample for the next antigen detection. These steps of primary antibody incubation, secondary antibody detection, and fluorescence signal removal are repeated until all target antigens have been detected. Finally, the nuclei are stained using DAPI, and the sections are mounted with an antifade mounting medium. Multichannel images are captured using a fluorescence microscope, and the multiple fluorescence signals are analyzed quantitatively and qualitatively using image analysis software. Through these steps, multiple target antigens can be detected and analyzed within the same tissue sample, providing rich biological information. Immunohistochemistry (IHC) staining was assessed using a semi-quantitative scoring method (H Score) based on staining intensity and the percentage of positively stained tumor cells. Staining intensity was graded as follows: 0 (negative), 1 (weak), 2 (moderate), and 3 (strong). The percentage of positively stained tumor cells was scored on a scale from 0 to 100%. The final IHC score was calculated by multiplying the staining intensity score by the percentage of positive tumor cells, yielding a composite score ranging from 0 to 300. This composite score was used to compare antigen expression levels across samples.

5.11 Mass cytometry

Anti-VHH antibodies for CAR-T cell detection were customized by Polaris Biology, China. Mass cytometry antibodies (CytoATLAS, Polaris Biology, China) are detailed in Supplementary Table 1. Cells were stained and acquired using a mass cytometer (StarionX1, Polaris Biology, China). Data were analyzed using FlowJo (BD Biosciences, USA) and Uniform Manifold Approximation and Projection (UMAP) for immune compartment overview and FlowSOM clustering for cell subtype identification.

5.12 Establishment of CDX models

For the tumorigenesis assay, 1×10^7 cancer cells were resuspended in a 1:3 PBS/hydrogel solution and subcutaneously injected into the flanks of 6-week-old female NOD.Cg-PrkdcscidIl2rtm1Wjl/SzJ (NCG) mice (Shanghai Model Organisms) to assess tumor growth. Mice were randomized into groups based on body weight and initial tumor volume. Tumor size and body weight were monitored biweekly, beginning one-week post-injection. Tumor volume was calculated using the formula: $V = (A \times B^2)/2$, where V represents the volume (mm^3), A is the length (mm), and B is the width (mm).

5.13 Establishment of PDX models

Female NCG mice (GemPharmatech LLC) were maintained under sterile conditions in an SPF barrier facility. To establish patient-derived xenograft (PDX) models, fresh tumor specimens were sectioned into approximately 3 mm × 3 mm × 3 mm pieces and implanted subcutaneously into the flanks of 4 to 5-week-old female NCG mice. Tumor growth was monitored biweekly by measuring tumor dimensions. Once tumors reached 100 mm^3, they were excised, minced with scissors, and processed for further use. Tumor fragments were either re-implanted into NSG mice or preserved in 90% FBS and 10% DMSO for cryopreservation in liquid nitrogen. Additional fragments were utilized

for histopathological and molecular analyses. PDX models with successful engraftment were passaged and preserved following at least two generations in NCG mice. The further experiment was conducted when the tumor reaches 200 mm^3.

5.14 Murine syngeneic Panc02-m18.2 model

Panc02-m18.2 tumor cells were harvested with 0.05% trypsin, washed, and resuspended in PBS for injection. A total of 4×10^6 tumor cells were subcutaneously inoculated into the flanks of 6–8-week-old C57BL/6 mice. Eight days later, when the tumors averaged 20–40 mm^3 in volume, mice received cyclophosphamide and were subsequently assigned to experimental groups ($n \geq 5$ per group) for comparison of tumor growth. On days 9 and 11, each group was administered 4×10^6 CAR-T cells or control T cells via intravenous injection. Tumor progression was monitored closely, with measurements of tumor length (L; the longest dimension) and width (W; the widest dimension) taken every 2–3 days using calipers. Tumor volume (V) was calculated with the formula: $V = (L \times W^2)/2$. Mice were euthanized either when tumors reached 1000 mm^3 or earlier if they exhibited signs of distress or morbidity, in accordance with ethical guidelines.

5.15 Statistical analysis

All statistical analyses were performed using GraphPad Prism software (GraphPad). Data points represent biological replicates and are shown as the mean ± SEM or mean ± SD as indicated in the figure legends. Statistical significance was determined using an unpaired two-tailed Student's t-test or two-way ANOVA. Significance was assumed with $*p < 0.05$; $**p < 0.01$; $***p < 0.001$.

Supplementary Information The online version contains supplementary material available at https://doi.org/10.1007/s13402-025-01066-5.

Acknowledgments We thank Yuhan Wang, Dr. Shijia Wang, and Dr. Xinzhu Wang from Polaris Biology, Shanghai for the performance of the mass cytometry experiment and analysis data.

Author contributions MS, YC, XZ, HX, and RH designed in vitro and in vivo experiments; MS, LB, HW, XL, and YL performed in vitro and in vivo experiments; MS, RH, BZ and SZ collected and analyzed data; YZ constructed plasmids and lentiviral vector; MS, LB, RH, HW, HX, XZ and YC wrote the manuscript.

Funding This study is sponsored by Immunofoco Biotechnology.

Data availability No datasets were generated or analysed during the current study.

Declarations

Ethics approval All animal protocols and procedures were approved by the by the Institutional Animal Care and Use Committee of Shanghai Model Organisms Center (2022-0049).

Declaration of interests MS, RH, YL, YZ and SZ are employees of Suzhou Immunofoco Biotechnology Co., Ltd.; LB, HW, XL, HX, XZ, YC reports consulting, advisory role, or receive research funding from Immunofoco.

Competing interests The authors declare no competing interests.

References

1. N. Denlinger, D. Bond, S. Jaglowski, CAR T-cell therapy for B-cell lymphoma. Curr. Probl. Cancer. **46**(1), 100826 (2022). https://doi.org/10.1016/j.currproblcancer.2021.100826
2. D. Han, Z. Xu, Y. Zhuang, et al., Current progress in CAR-T cell therapy for hematological malignancies. J. Cancer **12**(2), 326–334 (2021). https://doi.org/10.7150/jca.48976
3. S. Ma, X. Li, X. Wang, et al., Current progress in CAR-T cell therapy for solid tumors. Int. J. Biol. Sci. **15**(12), 2548–2560 (2019). https://doi.org/10.7150/ijbs.34213
4. C.E. Meacham, S.J. Morrison, Tumour heterogeneity and cancer cell plasticity. Nature **501**(7467), 328–337 (2013). https://doi.org/10.1038/nature12624
5. A. Klampatsa, M.S. Leibowitz, J. Sun, et al., Analysis and augmentation of the immunologic bystander effects of CAR T cell therapy in a syngeneic mouse cancer model. Mol Ther Oncolytics **18**, 360–371 (2020). https://doi.org/10.1016/j.omto.2020.07.005
6. P.R. Prasetyanti, J.P. Medema, Intra-tumor heterogeneity from a cancer stem cell perspective. Mol Cancer **16**(1), 41 (2017). https://doi.org/10.1186/s12943-017-0600-4
7. M. Dottermusch, S. Kruger, H.M. Behrens, et al., Expression of the potential therapeutic target claudin-18.2 is frequently decreased in gastric cancer: results from a large Caucasian cohort study. Virchows Arch. **475**(5), 563–571 (2019). https://doi.org/10.1007/s00428-019-02624-7
8. U. Sahin, M. Koslowski, K. Dhaene, et al., Claudin-18 splice variant 2 is a pan-cancer target suitable for therapeutic antibody development. Clin. Cancer. Res. **14**(23), 7624–7634 (2008). https://doi.org/10.1158/1078-0432.CCR-08-1547
9. W. Cao, H. Xing, Y. Li, et al., Claudin18.2 is a novel molecular biomarker for tumor-targeted immunotherapy. Biomark Res **10**(1), 38 (2022). https://doi.org/10.1186/s40364-022-00385-1

10. J.H. Baek, D.J. Park, G.Y. Kim, et al., Clinical implications of claudin18.2 expression in patients with gastric cancer. Anticancer Res. **39**(12), 6973–6979 (2019). https://doi.org/10.21873/anticanres.13919
11. C. Qi, J. Gong, J. Li, et al., Claudin18.2-specific CAR T cells in gastrointestinal cancers: phase 1 trial interim results. Nat. Med. **28**(6), 1189–1198 (2022). https://doi.org/10.1038/s41591-022-01800-8
12. C. Rohde, R. Yamaguchi, S. Mukhina, et al., Comparison of Claudin 18.2 expression in primary tumors and lymph node metastases in Japanese patients with gastric adenocarcinoma. Jpn. J. Clin. Oncol. **49**(9), 870–876 (2019). https://doi.org/10.1093/jjco/hyz068
13. P. Micke, J.S. Mattsson, K. Edlund, et al., Aberrantly activated claudin 6 and 18.2 as potential therapy targets in non-small-cell lung cancer. Int. J. Cancer **135**(9), 2206–2214 (2014). https://doi.org/10.1002/ijc.28857
14. J.Y. Hong, J.Y. An, J. Lee, et al., Claudin 18.2 expression in various tumor types and its role as a potential target in advanced gastric cancer. Transl. Cancer Res. **9**(5), 3367–3374 (2020). https://doi.org/10.21037/tcr-19-1876
15. U. Sahin, M. Schuler, H. Richly, et al., A phase I dose-escalation study of IMAB362 (Zolbetuximab) in patients with advanced gastric and gastro-oesophageal junction cancer. Eur J Cancer **100**, 17–26 (2018). https://doi.org/10.1016/j.ejca.2018.05.007
16. O. Tureci, U. Sahin, H. Schulze-Bergkamen, et al., A multicentre, phase IIa study of zolbetuximab as a single agent in patients with recurrent or refractory advanced adenocarcinoma of the stomach or lower oesophagus: the MONO study. Ann. Oncol. **30**(9), 1487–1495 (2019). https://doi.org/10.1093/annonc/mdz199
17. L.I. Ehrlich, K. Ogasawara, J.A. Hamerman, et al., Engagement of NKG2D by cognate ligand or antibody alone is insufficient to mediate costimulation of human and mouse CD8+ T cells. J Immunol **174**(4), 1922–1931 (2005). https://doi.org/10.4049/jimmunol.174.4.1922
18. C. Perez, K. Prajapati, B. Burke, et al., NKG2D signaling certifies effector CD8 T cells for memory formation. J Immunother Cancer **7**(1), 48 (2019). https://doi.org/10.1186/s40425-019-0531-2
19. K. Prajapati, C. Perez, L.B.P. Rojas, et al., Functions of NKG2D in CD8(+) T cells: an opportunity for immunotherapy. Cell Mol Immunol **15**(5), 470–479 (2018). https://doi.org/10.1038/cmi.2017.161
20. S. Gasser, S. Orsulic, E.J. Brown, et al., The DNA damage pathway regulates innate immune system ligands of the NKG2D receptor. Nature **436**(7054), 1186–1190 (2005). https://doi.org/10.1038/nature03884
21. R.A. Eagle, J.A. Traherne, O. Ashiru, et al., Regulation of NKG2D ligand gene expression. Hum. Immunol. **67**(3), 159–169 (2006). https://doi.org/10.1016/j.humimm.2006.02.015
22. H. Liu, S. Wang, J. Xin, et al., Role of NKG2D and its ligands in cancer immunotherapy. Am J Cancer Res **9**(10), 2064–2078 (2019).
23. P. Dhar, J.D. Wu, NKG2D and its ligands in cancer. Curr Opin Immunol **51**, 55–61 (2018). https://doi.org/10.1016/j.coi.2018.02.004
24. D. Garrity, M.E. Call, J. Feng, et al., The activating NKG2D receptor assembles in the membrane with two signaling dimers into a hexameric structure. Proc. Natl. Acad. Sci. U. S. A. **102**(21), 7641–7646 (2005). https://doi.org/10.1073/pnas.0502439102
25. D.D. Billadeau, J.L. Upshaw, R.A. Schoon, et al., NKG2D-DAP10 triggers human NK cell-mediated killing via a Syk-independent regulatory pathway. Nat Immunol **4**(6), 557–564 (2003). https://doi.org/10.1038/ni929
26. D.B. Graham, M. Cella, E. Giurisato, et al., Vav1 controls DAP10-mediated natural cytotoxicity by regulating actin and microtubule dynamics. J Immunol **177**(4), 2349–2355 (2006). https://doi.org/10.4049/jimmunol.177.4.2349
27. J.L. Upshaw, L.N. Arneson, R.A. Schoon, et al., NKG2D-mediated signaling requires a DAP10-bound Grb2-Vav1 intermediate and phosphatidylinositol-3-kinase in human natural killer cells. Nat Immunol **7**(5), 524–532 (2006). https://doi.org/10.1038/ni1325
28. L.L. Lanier, B.C. Corliss, J. Wu, et al., Immunoreceptor DAP12 bearing a tyrosine-based activation motif is involved in activating NK cells. Nature **391**(6668), 703–707 (1998). https://doi.org/10.1038/35642
29. D.B. Rosen, M. Araki, J.A. Hamerman, et al., A Structural basis for the association of DAP12 with mouse, but not human, NKG2D. J Immunol **173**(4), 2470–2478 (2004). https://doi.org/10.4049/jimmunol.173.4.2470
30. Y.Y. Ng, J.C.K. Tay, Z. Li, et al., T cells expressing NKG2D CAR with a DAP12 signaling domain stimulate lower cytokine production while effective in tumor eradication. Mol Ther **29**(1), 75–85 (2021). https://doi.org/10.1016/j.ymthe.2020.08.016
31. T. Zhang, C.L. Sentman, Mouse tumor vasculature expresses NKG2D ligands and can be targeted by chimeric NKG2D-modified T cells. J Immunol **190**(5), 2455–2463 (2013). https://doi.org/10.4049/jimmunol.1201314
32. N. Nausch, I.E. Galani, E. Schlecker, et al., Mononuclear myeloid-derived "suppressor" cells express RAE-1 and activate natural killer cells. Blood **112**(10), 4080–4089 (2008). https://doi.org/10.1182/blood-2008-03-143776
33. J. Obajdin, D. Larcombe-Young, M. Glover, et al., Solid tumor immunotherapy using NKG2D-based adaptor CAR T cells. Cell Rep Med **5**(11), 101827 (2024). https://doi.org/10.1016/j.xcrm.2024.101827
34. M. Champsaur, L.L. Lanier, Effect of NKG2D ligand expression on host immune responses. Immunol. Rev. **235**(1), 267–285 (2010). https://doi.org/10.1111/j.0105-2896.2010.00893.x

Authors and Affiliations

Minmin Sun[1,2,3,4] · Linke Bian[5,6] · Hongye Wang[5,6] · Xin Liu[1] · Yantao Li[3,4] · Zhaorong Wu[5,6] · Shuangshuang Zhang[3,4] · Ruidong Hao[3,4] · Hong Xin[1] · Bo Zhai[7] · Xuemei Zhang[1,2] · Yuanguo Cheng[1,2,3]

✉ Linke Bian
linked.bian@outlook.com

Hong Xin
xinhong@fudan.edu.cn

Bo Zhai
zhaiboshi@sina.com

Xuemei Zhang
xuemzhang@fudan.edu.cn

Yuanguo Cheng
yuanguo.cheng@immunofoco.com

[1] School of Pharmacy, Fudan University, Shanghai, P.R. China

[2] China State Institute of Pharmaceutical Industry, Shanghai, P.R. China

[3] Suzhou Immunofoco Biotechnology Co., Ltd., Jiangsu, P.R. China

[4] Shanghai Immunofoco Biotech Research Co., Ltd., Shanghai, P.R. China

[5] Department of Interventional Oncology, Renji Hospital, Shanghai Jiao Tong University School of Medicine, Shanghai, China

[6] State Key Laboratory of Oncogenes and Related Genes, Shanghai Cancer Institute, Renji Hospital, Shanghai Jiao Tong University School of Medicine, Shanghai, China

[7] Mini-invasive Interventional Therapy Center, Shanghai East Hospital, Tongji University, Shanghai 200025, China